UDC 621.319 https://doi.org/10.20998/2074-272X.2025.4.06

I. Kovacova, D. Kovac

Designing the optimal number of active branches in a multi-branch buck-boost converter

Introduction. *Multi-branch buck-boost converters, widely used in energy conversion from alternative sources, offer significant advantages over single-branch configurations. Critical, however, is the question of the appropriate number of branches for optimal efficiency and the given output power of the converter.* ***The novelty*** *of the proposed work consists in the development of a precise method for determining the optimal number of branches in a multi-branch buck-boost converter for a specified output power. Additionally, the findings enable the development of adaptive control strategies that dynamically adjust the number of active branches based on the converter's instantaneous power. This approach enhances the overall efficiency of the converter.* ***Goal.*** *The study aims to analyze the efficiency of multi-branch buck-boost converters, focusing on the optimal number of branches and the required output power.* ***Methods.*** *The problem was addressed through a theoretical analysis of the converter's electrical equivalent circuit. The theoretical results were validated through practical measurements conducted on a prototype converter.* ***Results.*** *A detailed equivalent circuit for the converter was developed and analyzed for various operational modes. Based on this analysis, the converter's losses were quantified, and a relationship was derived to determine the optimal number of parallel branches, taking into account the desired output power.* ***Practical value.*** *The findings provide guidelines for selecting the optimal number of branches in a multi-branch buck-boost converter based on the desired output power. Furthermore, they enable the implementation of adaptive switching strategies to maximize the converter's efficiency.* References 22, table 2, figures 20.
Key words: **multi-branch buck-boost converter, power losses, efficiency.**

Вступ. *Багатогілкові понижувально-підвищувальні перетворювачі, що широко використовуються в перетворенні енергії з альтернативних джерел, пропонують значні переваги порівняно з одногілковими конфігураціями. Однак критичним є питання відповідної кількості гілок для оптимальної ефективності та заданої вихідної потужності перетворювача.* ***Новизна*** *запропонованої роботи полягає в розробці точного методу визначення оптимальної кількості гілок у багатогілковому понижувально-підвищувальному перетворювачі для заданої вихідної потужності. Крім того, отримані результати дозволяють розробляти адаптивні стратегії керування, які динамічно регулюють кількість активних гілок на основі миттєвої потужності перетворювача. Такий підхід підвищує загальну ефективність перетворювача.* ***Метою*** *дослідження є аналіз ефективності багатогілкових понижувально-підвищувальних перетворювачів, зосереджуючись на оптимальній кількості гілок та необхідній вихідній потужності.* ***Методи***. *Проблему вирішено за допомогою теоретичного аналізу електричної еквівалентної схеми перетворювача. Теоретичні результати перевірені за допомогою практичних вимірювань, проведених на прототипі перетворювача.* ***Результати***. *Була розроблена та проаналізована детальна еквівалентна схема перетворювача для різних режимів роботи. На основі цього аналізу було кількісно визначено втрати перетворювача та виведено співвідношення для визначення оптимальної кількості паралельних гілок з урахуванням бажаної вихідної потужності.* ***Практична значимість***. *Отримані результати надають рекомендації щодо вибору оптимальної кількості гілок у багатогілковому понижувально-підвищувальному перетворювачі на основі бажаної вихідної потужності. Крім того, вони дозволяють реалізувати адаптивні стратегії перемикання для максимізації ефективності перетворювача.* Бібл. 22, табл. 2, рис. 20.
Ключові слова: **багатогілковий понижувально-підвищувальний перетворювач, втрати потужності, ефективність.**

Introduction. Multi-branch DC/DC converters offer several advantages over their single-branch counterparts. Key benefits include significantly reduced output current ripple at the same switching frequency [1–4], a narrower range of operation in discontinuous current modes [5–8], and increased energy conversion efficiency from input to output [9–11]. This is achieved by eliminating operational intervals where energy is merely stored within the converter without being transferred to the output.

However, the optimal number of active branches in these multi-branch configurations remains an open question [12, 13]. The study **aims** to analyze the efficiency of multi-branch buck-boost converters, focusing on the optimal number of branches and the required output power. Addressing this issue requires an analysis focused on maximizing the converter's efficiency. Therefore, the subsequent sections provide a detailed analysis of the calculation for the optimal number of active branches, considering both buck and boost operating modes. The topology of such a converter is illustrated in Fig. 1.

Analysis of buck-boost converter operation in buck mode and associated losses. The configuration of the analyzed converter operating in step-down (buck) mode with *n* branches is shown in Fig. 2 [14–16]. In this case, the second transistor for the *n*-th branch is not considered.

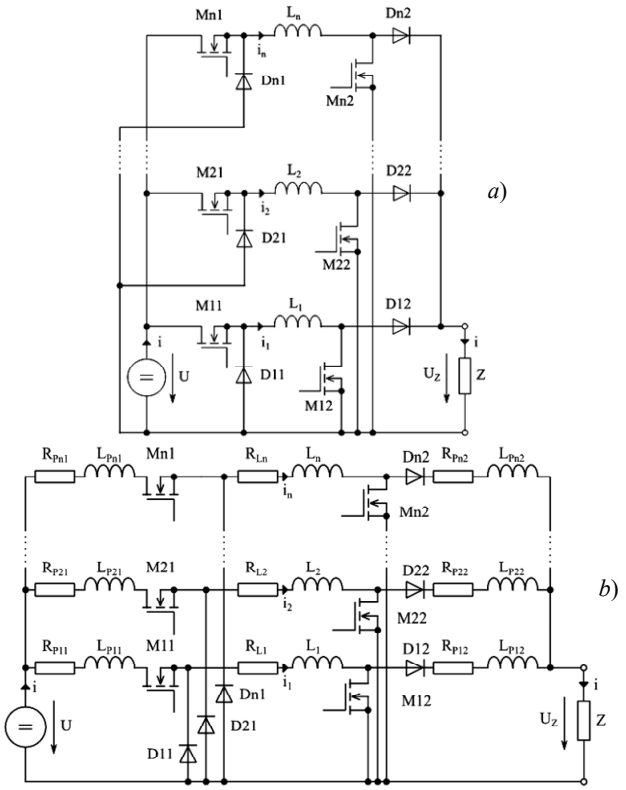

Fig. 1. Circuit diagram of the *n*-branch buck-boost converter
a) principle design; *b*) including parasitic elements

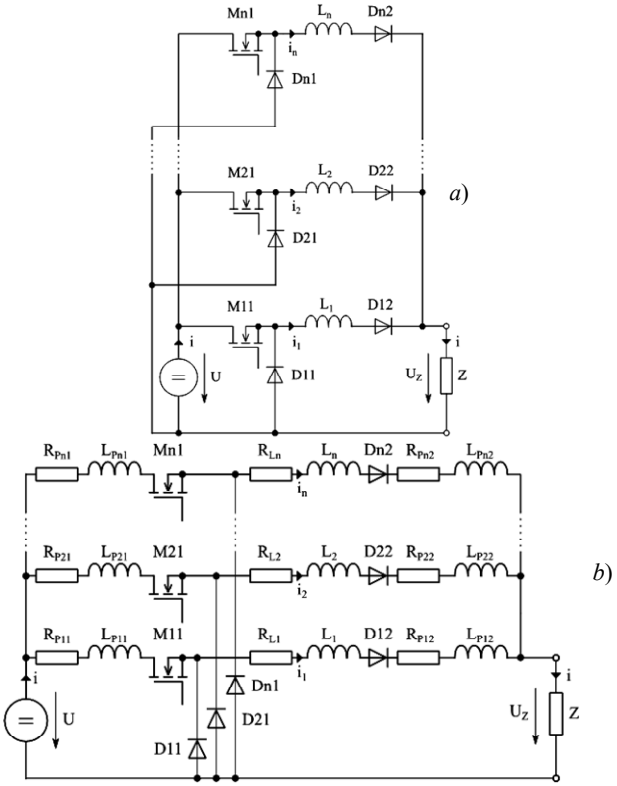

Fig. 2. Configuration of the *n*-branch buck-boost converter in buck mode:
a) fundamental design; *b*) including parasitic elements

All components in the circuit diagram marked with the index *p* represent the parasitic elements of the circuit. According to the 1st Kirchhoff's law (KCL), the currents in the circuit satisfy the equation (1):

$$i = \sum_{j=1}^{n} i_j \ . \tag{1}$$

Each branch of the converter operates with identical switching behavior, but the control signals for individual branches are time-shifted relative to each other by an interval of T/n, where T is the switching period and n is the number of branches in the converter [17–19]. Fundamentally, the operation of each branch can be divided into two primary intervals.

1st Interval. During this phase of operation, the transistor in the branch is switched on, allowing energy to accumulate in the circuit's main inductance, which is supplied by the input voltage source with a value of U. This scenario is illustrated in Fig. 3.

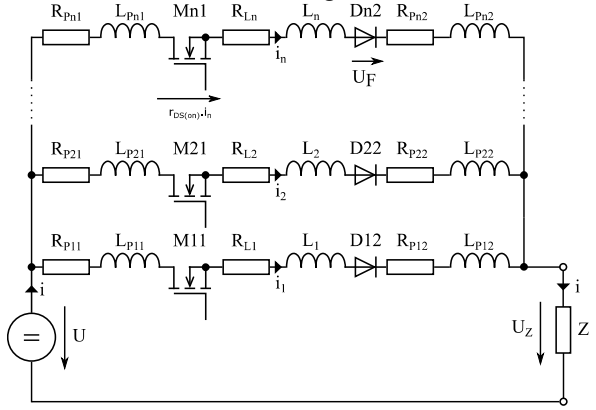

Fig. 3. Equivalent circuit for the first operational interval of the converter

For the *n*-th conductive loop of the converter, the equation can be written according to Kirchhoff's voltage law (KVL):

$$\begin{aligned} &-U + R_{Pn1} i_n + L_{Pn1} \frac{\mathrm{d}i_n}{\mathrm{d}t} + r_{DS(on)n} i_n + R_{Ln} i_n + \\ &+ L_n \frac{\mathrm{d}i_n}{\mathrm{d}t} + U_F + R_{Pn2} i_n + L_{Pn2} \frac{\mathrm{d}i_n}{\mathrm{d}t} + U_Z = 0, \end{aligned} \tag{2}$$

where U is the input voltage; R_{Pn1} is the resistance of the supply conductor; L_{Pn1} is the parasitic inductance of the supply conductor; $r_{\mathrm{DS(on)}}$ is the resistance of the MOSFET transistor in the on-state; R_{Ln} is the resistance of the main inductor; L_{n} is the inductance of the main inductor; U_{F} is the voltage drop across the diode; R_{Pn2} is the resistance of the conductor leading to the load; U_{Z} is the voltage across the load.

Since the described circuit contains only an ohmic-inductive load, the current waveform will take the form depicted in Fig. 4.

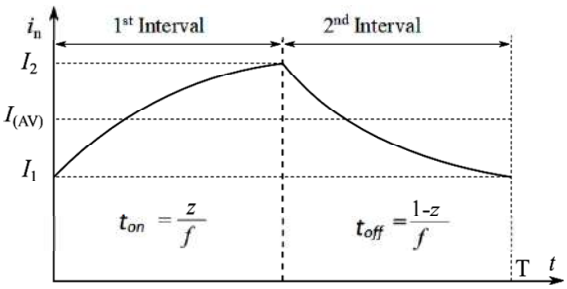

Fig. 4. Current waveform in the *n*-th branch

The *n*-th loop of the converter, shown in Fig. 3, can be simplified by concentrating the parameters:

$$U_Z = Z \cdot i = Z \cdot \sum_{i=1}^{n} i_i = Z \cdot n \cdot i_n \, ; \tag{3}$$

$$U_F = U_{TO} + r_F i_n \, ; \tag{4}$$

$$R_{n1} = R_{Pn1} + r_{DS(on)} + R_{Ln} + R_{Pn2} + r_F \, ; \tag{5}$$

$$L_{n1} = L_{Pn1} + L_n + L_{Pn2} \, , \tag{6}$$

where U_{TO} is the threshold voltage across the diode; Z is the magnitude of the load impedance; R_{n1} is the resistance of the *n*-th branch during the first interval; r_{F} is the forward resistance of the diode; L_{n1} is the inductance of the *n*-th branch during the first interval.

By considering (3) through (6), the initial equation (2) takes the following form:

$$U_{TO} - U + Z \cdot n \cdot i_n + R_{n1} i_n + L_{n1} \frac{\mathrm{d}i_n}{\mathrm{d}t} = 0 \, . \tag{7}$$

The solution to this equation, expressing the current i_n, is obtained as follows:

$$i_n = \frac{U - U_{TO}}{(R_{n1} + nZ)} \left(1 - e^{-\frac{(R_{n1}+nZ)}{L_{n1}} t} \right) + I_1 e^{-\frac{(R_{n1}+nZ)}{L_{n1}} t} \, . \tag{8}$$

If, in this temporal expression of current, the time t is substituted with $t = t_{on} = z/f$, then at this specific moment, the current i_n, as shown in Fig. 4, assumes the value I_2:

$$I_2 = \frac{U - U_{TO}}{(R_{n1} + nZ)} \left(1 - e^{-\frac{(R_{n1}+nZ)}{L_{n1}} \cdot \frac{z}{f}} \right) + I_1 e^{-\frac{(R_{n1}+nZ)}{L_{n1}} \cdot \frac{z}{f}} \, , \tag{9}$$

where z is the pulse width (duty cycle) of the converter's control; f denotes its switching frequency.

2nd Interval. During the 2nd operational interval of the converter, the transistor is switched off, allowing the energy stored in the inductance L_n to be transferred to the load through diodes D_{n1} and D_{n2} (Fig. 5).

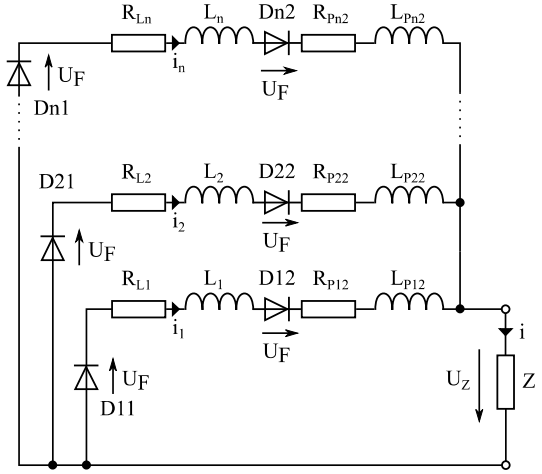

Fig. 5. Equivalent circuit diagram for the second operational interval of the converter

For the n-th conductive loop of the converter, the equation can be formulated based on KVL as follows:

$$U_Z + U_F + R_{Ln} i_n + L_n \frac{\mathrm{d}i_n}{\mathrm{d}t} + U_F + R_{Pn2} i_n + L_{Pn2} \frac{\mathrm{d}i_n}{\mathrm{d}t} = 0, \quad (10)$$

where equation (3) applies, along with the following equations:

$$R_{n2} = R_{Ln} + 2r_F + R_{Pn2}; \quad (11)$$

$$L_{n2} = L_n + L_{Pn2}. \quad (12)$$

Based on the information provided above, a modified version of (10) can be derived:

$$nZi_n + 2U_{TO} + R_{n2} i_n + L_{n2} \frac{\mathrm{d}i_n}{\mathrm{d}t} = 0. \quad (13)$$

Solving the equation yields the time-dependent behavior of the desired current i_n, which is expressed by the following formula:

$$i_n = \frac{-2U_{TO}}{(R_{n2}+nZ)} \left(1 - e^{-\frac{(R_{n2}+nZ)}{L_{n2}} t}\right) + I_2 e^{-\frac{(R_{n2}+nZ)}{L_{n2}} t}. \quad (14)$$

Substituting the value of time $t = t_{off} = (1–z)/f$ into the equation provides, as illustrated in Fig. 4, the expression for the current i_n with a magnitude of I_1:

$$I_1 = \frac{-2.U_{TO}}{(R_{n2}+nZ)} \left(1 - e^{-\frac{(R_{n2}+nZ)}{L_{n2}} \cdot \frac{(1-z)}{f}}\right) + I_2 e^{-\frac{(R_{n2}+nZ)}{L_{n2}} \cdot \frac{(1-z)}{f}}. \quad (15)$$

Based on (9) and (15), it is possible to derive expressions for the initial values of currents I_1 and I_2 at the beginning of both intervals of the converter. These values are determined solely by the circuit parameters. The value of current I_2 from (9) is substituted into (15), resulting in the following expression:

$$I_1 = \frac{-2.U_{TO}}{(R_{n2}+nZ)} \left(1 - e^{-\frac{(R_{n2}+nZ)}{L_{n2}} \cdot \frac{(1-z)}{f}}\right) + \left(\frac{U - U_{TO}}{(R_{n1}+nZ)} \left(1 - e^{-\frac{(R_{n1}+nZ)}{L_{n1}} \cdot \frac{z}{f}}\right) + I_1 e^{-\frac{(R_{n1}+nZ)}{L_{n1}} \cdot \frac{z}{f}}\right) e^{-\frac{(R_{n2}+nZ)}{L_{n2}} \cdot \frac{(1-z)}{f}}. \quad (16)$$

The final expression for the current I_1 value is obtained after manipulating (16) in the following form:

$$I_1 = \frac{\left(\frac{-2U_{TO}}{(R_{n2}+nZ)} \left(1 - e^{-\frac{(R_{n2}+nZ)}{L_{n2}} \cdot \frac{(1-z)}{f}}\right) + \left(\frac{U - U_{TO}}{(R_{n1}+nZ)} \left(1 - e^{-\frac{(R_{n1}+nZ)}{L_{n1}} \cdot \frac{z}{f}}\right) e^{-\frac{(R_{n2}+nZ)}{L_{n2}} \cdot \frac{(1-z)}{f}}\right)\right)}{\left(1 - e^{-\frac{(R_{n1}+nZ)}{L_{n1}} \cdot \frac{z}{f}} \cdot e^{-\frac{(R_{n2}+nZ)}{L_{n2}} \cdot \frac{(1-z)}{f}}\right)}. \quad (17)$$

The magnitude of the current I_2 is determined by substituting (17) into (9):

$$I_2 = \frac{U - U_{TO}}{(R_{n1}+nZ)} \left(1 - e^{-\frac{(R_{n1}+n.Z)}{L_{n1}} \cdot \frac{z}{f}}\right) + \frac{\left(\frac{-2U_{TO}}{(R_{n2}+nZ)} \left(1 - e^{-\frac{(R_{n2}+nZ)}{L_{n2}} \cdot \frac{(1-z)}{f}}\right) + \left(\frac{U - U_{TO}}{(R_{n1}+nZ)} \left(1 - e^{-\frac{(R_{n1}+nZ)}{L_{n1}} \cdot \frac{z}{f}}\right) e^{-\frac{(R_{n2}+nZ)}{L_{n2}} \cdot \frac{(1-z)}{f}}\right)\right)}{\left(\frac{1}{e^{\frac{(R_{n1}+nZ)}{L_{n1}} \cdot \frac{z}{f}}} - e^{-\frac{(R_{n2}+nZ)}{L_{n2}} \cdot \frac{(1-z)}{f}}\right)}. \quad (18)$$

Based on (8), (14), (17), (18), the time-dependent current through any branch of a multi-phase buck-boost converter can be expressed.

However, determining the optimal number of branches for the converter also requires calculating the total losses in the system as a function of the number of branches. These losses are categorized into steady-state losses, occurring during both operating intervals, and dynamic losses, arising during transient processes. The composition and notation for these losses are as follows:

Steady-state losses:

P_{RPn1} – losses due to the resistance of the input conductor in the n^{th} branch.

P_{MF} – losses on the MOSFET transistor in the ON state.

P_{MR} – losses on the MOSFET transistor in the OFF state.

P_{RLn} – losses due to the resistance of the inductor in the n^{th} branch.

P_{DF} – losses on the diode in the ON state.

P_{DR} – losses on the diode in the OFF state.

P_{RPn2} – losses due to the resistance of the output conductor in the n^{th} branch.

Dynamic losses:

P_{Mon} – switching losses on the MOSFET transistor during turn-on.

P_{Moff} – switching losses on the MOSFET transistor during turn-off.

P_{DQR} – switching losses on the diode during turn-off.

P_{DQF} – switching losses on the diode during turn-on.

Considering standard waveforms for the switching processes and using (1), the total losses P_C of the converter can be expressed as:

$$P_C = P_{RPn1} + P_{MF} + P_{MR} + P_{RLn} + P_{DF} + P_{DR} + P_{RPn2} + P_{Mon} + P_{Moff} + P_{DQR} + P_{DQF}. \quad (19)$$

The average value of the current in a branch of the converter can be determined as:

$$I_{n(AV)} = (I_1 + I_2)/2 = I/n, \quad (20)$$

where I is the average current of the converter. Based on this, the total losses of the converter can be expressed as:

$$\begin{aligned} P_C = {} & nR_{Pn1}\left(I_{n(AV)}\right)^2 z + nr_{DS(on)}\left(I_{n(AV)}\right)^2 z + nUI_{DS}(1-z) + \\ & + nR_{Ln}\left(I_{n(AV)}\right)^2 + 2n\left(U_{TO} + r_F\left(I_{n(AV)}\right)\right)I_{n(AV)}(1-z) + \\ & + n\left(U_{TO} + r_F\left(I_{n(AV)}\right)\right)I_{n(AV)}z + nUI_R z + nR_{Pn2}\left(I_{n(AV)}\right)^2 + \\ & + 0{,}5nUI_1 t_{on} f + 0{,}5nUI_2 t_f f + 0{,}5nQ_{rr}Uf + 0{,}5nU_{FP}I_2 t_{fr} f, \end{aligned} \quad (21)$$

where $r_{DS(on)}$ is the on-state resistance of the transistor; $r_{DS(off)}$ is the off-state resistance of the transistor; I_R is the reverse current flowing through the diode; $I_{DS(off)}$ is the current flowing through the transistor during its off-state; t_{on} is the time required for the MOSFET transistor to transition from the off-state to the on-state; t_f is the time required for the MOSFET to transition from the on-state to the off-state; Q_{rr} is the reverse recovery charge of the diode; U_{FP} is the voltage across the diode during its transition from the off-state to the on-state, governed by the time constant t_{fr}.

By reformulating (21) and applying (20), a simplified final form of the expression is obtained, enabling the calculation of the total losses within the converter [20]:

$$\begin{aligned} P_C = {} & \left(\frac{I^2}{n}\right)\cdot\left(R_{Pn1}z + r_{DS(on)}z + R_{Ln} + 2r_F(1-z) + r_F z + R_{Pn2}\right) + \\ & + nUI_{DS}(1-z) + 2U_{TO}I(1-z) + U_{TO}Iz + nUI_R.z + \\ & + 0{,}5nUI_1 t_{on} f + 0{,}5nUI_2 t_f f + 0{,}5nQ_{rr}Uf + 0{,}5nU_{FP}I_2 t_{fr} f. \end{aligned} \quad (22)$$

The efficiency of the converter can then be expressed by the following equation:

$$\eta = \frac{P_{output}}{P_{input}} = \frac{P_{input} - P_C}{P_{input}} = 1 - \frac{P_C}{P_{input}} = 1 - \frac{P_C}{UI}. \quad (23)$$

From (23), it is evident that overall efficiency is primarily influenced by the total power losses. These losses can be minimized through the careful selection of individual circuit components. Additionally, the total losses can be further influenced by the number of parallel branches in the converter, as the input current is distributed linearly among the branches, while resistive losses decrease quadratically. As a result, converters with multiple branches may exhibit lower overall losses compared to a single-branch configuration. However, due to the additional losses introduced by the parallel branches, the assertion that increasing the number of branches always reduces losses does not hold true universally.

Consequently, determining the optimal number of branches for a given input power requirement becomes essential (assuming constant input voltage, desired input current, and a fixed duty cycle). The converter can be dynamically managed by adjusting its topology and duty cycle to achieve maximum efficiency for any given input power level. This optimization assumes fixed construction parameters and characteristics of the converter components.

To determine the optimal number of branches, equation (22) must be differentiated. By deriving this equation with respect to n, the number of branches, it is possible to identify the local extremum, which corresponds to the number of branches that minimizes the total power losses:

$$\begin{aligned} P'_C = {} & -\left(\frac{I^2}{n^2}\right)\cdot\left(R_{Pn1}z + r_{DS(on)}z + R_{Ln} + 2r_F(1-z) + r_F z + R_{Pn2}\right) + \\ & + UI_{DS}(1-z) + UI_R z + 0{,}5UI_1 t_{on} f + 0{,}5UI_2 t_f f + \\ & + 0{,}5Q_{rr}Uf + 0{,}5U_{FP}I_2 t_{fr} f. \end{aligned} \quad (24)$$

If the result of the differentiation is set equal to zero and solved for n, the equation takes the following form:

$$n = I \cdot \sqrt{\frac{\left(R_{Pn1}z + r_{DS(on)}z + R_{Ln} + \right.}{\left. + 2r_F(1-z) + r_F z + R_{Pn2}\right)}} \Bigg/ \sqrt{\left(\begin{array}{l} UI_{DS}(1-z) + UI_R z + 0{,}5UI_1 t_{on} f + \\ + 0{,}5UI_2 t_f f + 0{,}5Q_{rr}Uf + 0{,}5U_{FP}I_2 t_{fr} f \end{array}\right)}. \quad (25)$$

The above discussion indicates that, based on (25), the optimal number of branches for a buck-boost converter operating in buck mode can be determined using its design and operational parameters. This ensures that the converter delivers maximum power to the load under all operating conditions.

Experimental results. To verify the derived results, a single-branch and a three-branch buck-boost converter with resistive load R were implemented. The circuit diagram of the single-branch buck converter is shown in Fig. 6.

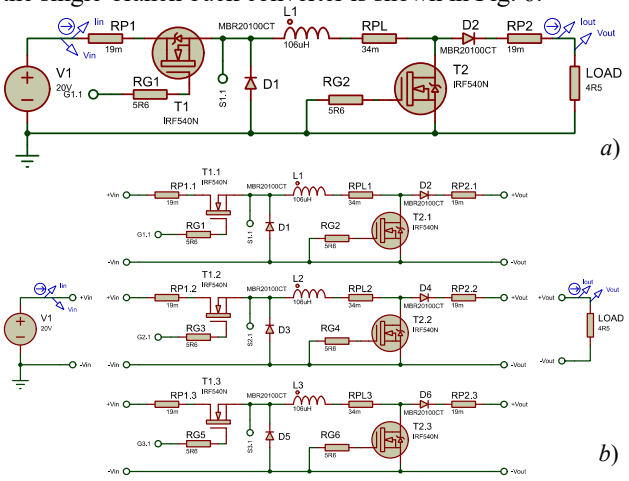

Fig. 6. Schematic of the implemented
a) 1-branch; *b*) 3-branches converter

The operational and design parameters of the converter are as follows: U=20 V, R_{pn1}=19 mΩ, L_{pn1}=1.5 μH, R_{Ln}=34 mΩ, L_n=106 μH, R_{pn2}=19 mΩ, L_{pn2}=0 H, $r_{DS(ON)}$=77 mΩ, I_{DS}=2.25 mA, t_{ON}=55 ns, t_f=96 ns, f=50 kHz, r_F=34 mΩ, U_{TO}=0.43 V, I_R=6 mA, Q_{rr}=0 C, U_{FP}=0 V, t_{fr}=2 ns, $Z = R$ = 4.5 Ω, The catalog data for the MOSFET IRF540N and the diode MBR20100CT were used in the implementation. The example of a practical implementation of the converter is shown in Fig. 7 [21].

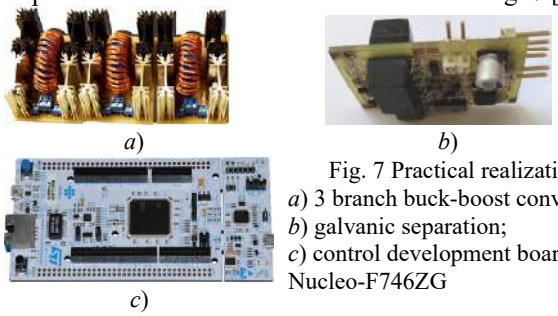

a) *b*)

Fig. 7 Practical realization:
a) 3 branch buck-boost converter;
b) galvanic separation;
c) control development board Nucleo-F746ZG

The waveforms of the measured main quantities for different input power levels (i.e., duty cycle values) and for different configurations of the number of phases are presented in Fig. 8 – 13. For all oscillograms, the following applies:
C1 – 900 mA/div: input current; C2 – 7 V/div: input voltage;
C3 – 900 mA/div: output current; C4 – 4 V/div: output voltage;
M1 – average input power; M2 – average output power;
M3 – average efficiency.

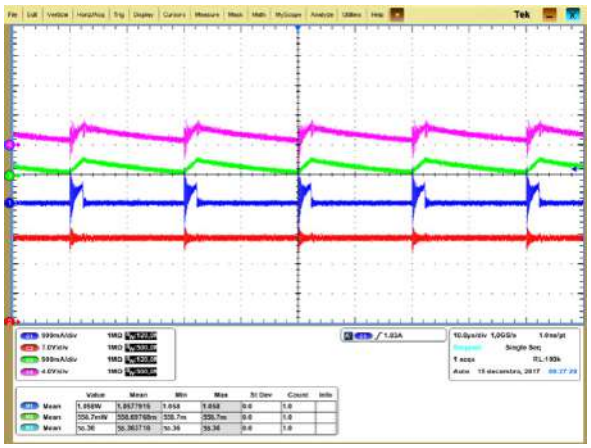

Fig. 8. Measured time waveforms of voltages and currents for the single-phase buck-boost converter in buck mode with 1 W input power

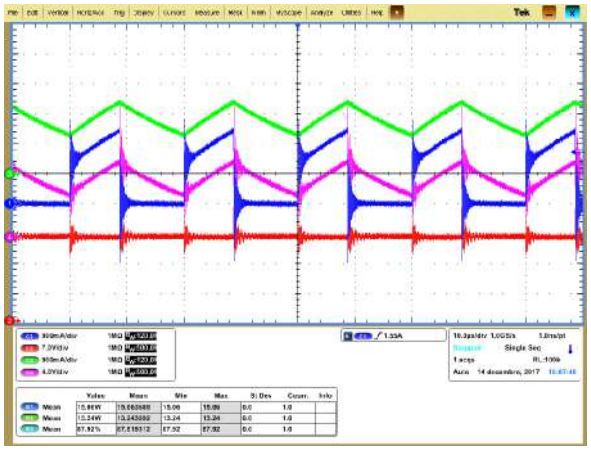

Fig. 9. Measured time waveforms of voltages and currents for the single-phase buck-boost converter in buck mode with 15 W input power

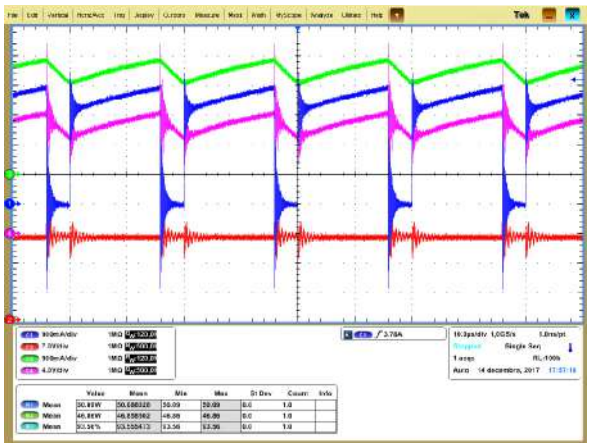

Fig. 10. Measured time waveforms of voltages and currents for the single-phase buck-boost converter in buck mode with 50 W input power

Based on the equations provided above and the parameters of the converter's equivalent circuit, the theoretical efficiency of the buck-boost converter in buck mode at a given power input can be calculated. The results obtained in this manner are presented in Table 1, where they are compared with the measurement results.

To provide a clearer understanding of the obtained results, graphs have been created (Fig. 14, 15).

Fig. 11. Measured time waveforms of voltages and currents for the three-phase buck-boost converter in buck mode with 1 W input power

Fig. 12. Measured time waveforms of voltages and currents for the three-phase buck-boost converter in buck mode with 15 W input power

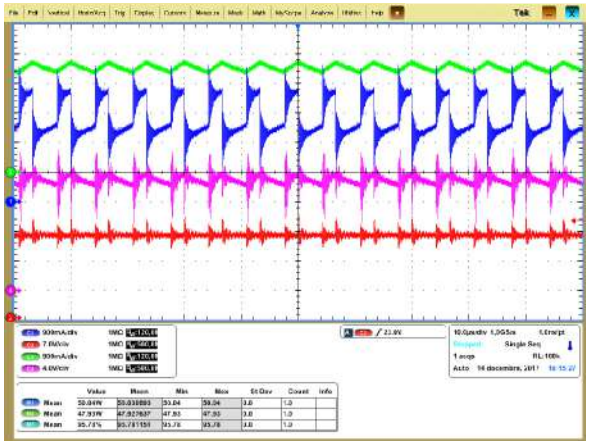

Fig. 13. Measured time waveforms of voltages and currents for the three-phase buck-boost converter in buck mode with 50 W input power

The comparison of results obtained through calculations, simulations, and measurements shows a sufficient agreement, indicating that the theoretically derived equations can be considered correct. The deviation between the calculated and measured efficiency values is less than 3 %. From this, it can be inferred that (22) is valid, and consequently, equation (25) for determining the optimal number of branches in a multi-branch buck-boost converter in the buck mode is also valid.

Table 1

Summary of results obtained from calculations and measurements

Single-phase converter in buck mode			
Calculated		Measured	
P_1, W	Efficiency, %	P_1, W	Efficiency, %
1,05	58,39	1,058	56,36
5,05	80,02	5,056	78,23
10,08	85,4	10,08	85,49
15,01	87,75	15,06	87,92
20	89,17	20,07	89,33
30	90,78	30,08	91,16
40	91,71	40,06	92,38
50,1	92,32	50,09	93,56
Three-phase converter in buck mode			
Calculated		Measured	
P_1, W	Efficiency, %	P_1, W	Efficiency, %
1,02	41,92	1,01	39,35
5	77,11	5	75,71
10,02	84,96	10,02	84,72
15,07	88,33	15,05	88,12
20,04	90,25	20,09	91,08
30,07	92,44	30,00	93,47
40,03	93,65	40,04	94,95
50	94,4	50,04	95,78

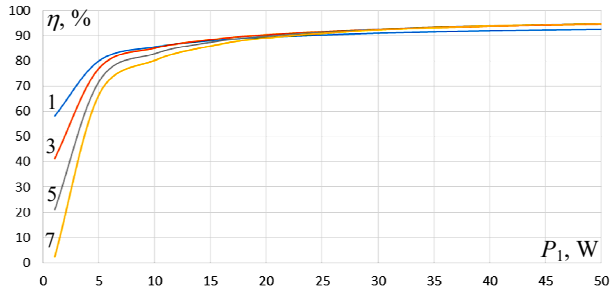

Fig. 14. Calculated efficiency of the converter as a function of input power and number of branches (1, 3, 5, 7)

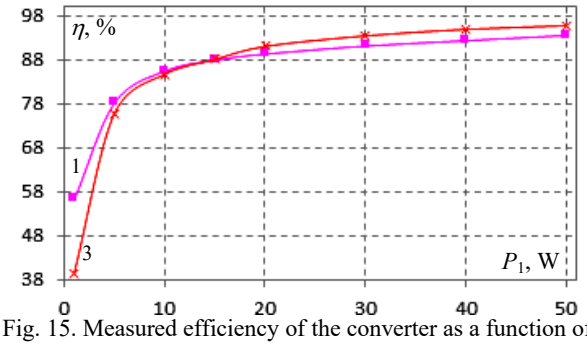

Fig. 15. Measured efficiency of the converter as a function of input power and number of branches (1, 3)

To illustrate the implications of the calculated results, Fig. 16 presents the computed dependence of the converter's efficiency on its output power for a higher-power converter. The implementation of this converter assumes the use of the following components: IRG4PH50S-EPbF and BYV29-500, alongside the circuit parameters: U=200 V, R_{pn1}=19 mΩ, L_{pn1}=1.5 μH, R_{Ln}=34 mΩ, L_n=330 μH, R_{pn2}=19 mΩ, L_{pn2}=1 μH, $r_{DS(ON)}$=47 mΩ, I_{DS}=1 mA, t_{ON}=61 ns, t_f=1270 ns, f=50 kHz, r_F=19 mΩ, U_{TO}=0.7 V, I_R=50 μA, Q_{rr}=40 nC, U_{FP}=2.5 V, t_{fr}=200 ns, $Z = R$ = 10 Ω.

The figure illustrates that the efficiency difference between the single-branch and seven-branch configurations of the 3 kW converter can reach up to 5 % at an output power of 500 W.

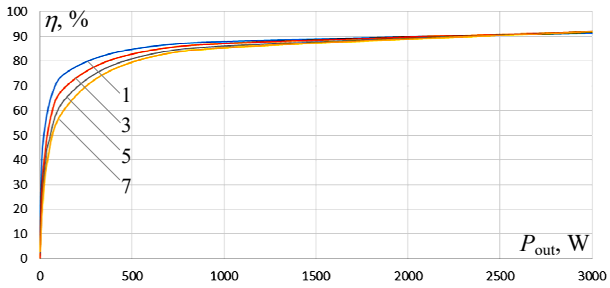

Fig. 16. Calculated efficiency of the higher power converter as a function of output power and number of branches (1, 3, 5, 7)

The next subsection presents the calculation of the optimal number of branches for the boost mode.

Analysis of the operation and losses in the boost mode of a buck-boost converter. The configuration of the analyzed multi-branch buck-boost converter in boost mode with n branches is shown in Fig. 1 [22]. Since the first transistor remains continuously open in this mode, its resistance in the closed state will be considered in the analysis of the converter.

All components in the circuit, indicated with the index p, represent parasitic elements. According to KCL, the equation (1) applies to the currents in the circuit.

Each branch of the converter operates similarly to the buck mode, where the control signals for the individual branches are time-shifted by T/n, with T being the switching period. The operation of each branch can be divided into two basic intervals.

1st Interval. During this operational interval, the transistor in the corresponding vertical branch is closed, causing energy to accumulate in the main inductance of the circuit, which is powered by the input voltage source with a value of U. This situation is depicted in Fig. 17.

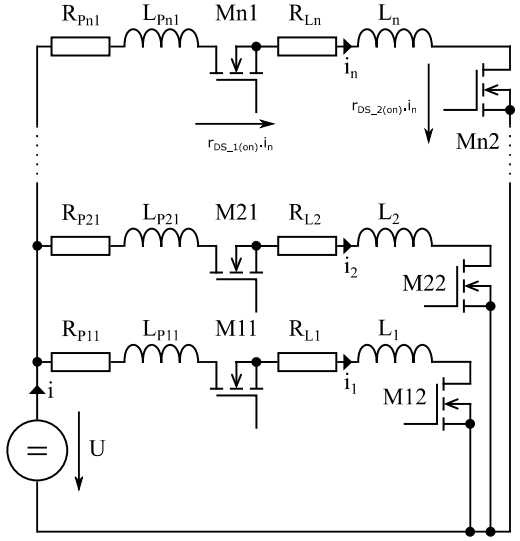

Fig. 17. Substitute diagram for the first operational interval of the converter in boost mode

For the n-th conductive loop of the converter, the equation can be formulated based on KVL as follows:

$$-U + R_{Pn1} \cdot i_n + L_{Pn1} \cdot \frac{\mathrm{d}i_n}{\mathrm{d}t} + r_{DS\_1(on)} \cdot i_n + R_{Ln} \cdot i_n + \\ + L_n \cdot \frac{\mathrm{d}i_n}{\mathrm{d}t} + r_{DS\_2(on)} \cdot i_n = 0. \quad (26)$$

The current waveform follows the same pattern as depicted in Fig. 4. The loop of the n-th branch of the converter, as shown in Fig. 17, can be simplified using lumped parameter modeling.

$$R_{n1} = R_{Pn1} + r_{DS\_1(on)} + R_{Ln} + r_{DS\_2(on)}; \quad (27)$$

$$L_{n1} = L_{Pn1} + L_n. \quad (28)$$

Considering (27) and (28), the initial equation (26) takes the following form:

$$-U + R_{n1} \cdot i_n + L_{n1} \cdot \frac{\mathrm{d}i_n}{\mathrm{d}t} = 0. \quad (29)$$

Its solution yields:

$$i_n = \frac{U}{R_{n1}} \cdot \left(1 - e^{-\frac{R_{n1}}{L_{n1}} \cdot t}\right) + I_1 \cdot e^{-\frac{R_{n1}}{L_{n1}} \cdot t}. \quad (30)$$

If the time variable $t = t_{on} = z/f$ is substituted into this time-dependent expression for the current, the current i_n at the specified moment will, as shown in Fig. 4, attain the value I_2:

$$I_2 = \frac{U}{R_{n1}} \cdot \left(1 - e^{-\frac{R_{n1}}{L_{n1}} \cdot \frac{z}{f}}\right) + I_1 \cdot e^{-\frac{R_{n1}}{L_{n1}} \cdot \frac{z}{f}}. \quad (31)$$

2nd Interval. In the 2nd operational interval of the buck-boost converter operation in boost mode, the transistor is switched off, and the energy stored in the inductance L_n is transferred to the load through the power supply and diode D_{n2}, as illustrated in Fig. 18.

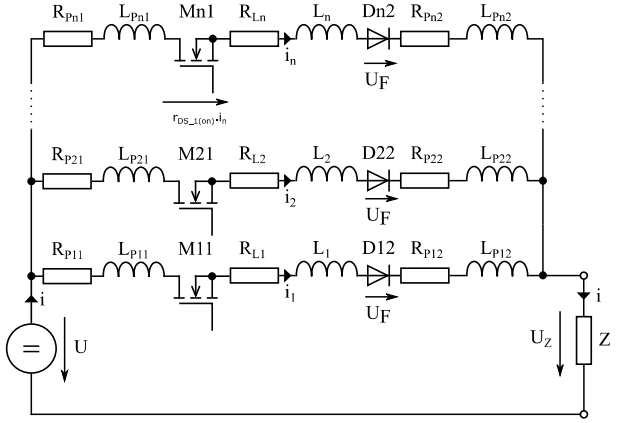

Fig. 18. Equivalent circuit for the second operational interval of the buck-boost converter in boost mode

For the n-th conductive loop of the converter, the equation can be written based on KVL as:

$$-U + R_{Pn1} \cdot i_n + L_{Pn1} \cdot \frac{\mathrm{d}i_n}{\mathrm{d}t} + r_{DS\_1(on)} \cdot i_n + R_{Ln} \cdot i_n + \\ + L_n \cdot \frac{\mathrm{d}i_n}{\mathrm{d}t} + U_F + R_{Pn2} \cdot i_n + L_{Pn2} \cdot \frac{\mathrm{d}i_n}{\mathrm{d}t} + U_Z = 0, \quad (32)$$

where (3) and the following equations hold:

$$R_{n2} = R_{Pn1} + r_{DS\_1(on)} + R_{Ln} + r_F + R_{Pn2}; \quad (33)$$

$$L_{n2} = L_{Pn1} + L_n + L_{Pn2}. \quad (34)$$

Based on the above, the modified version of (32) can be derived.

$$-U + R_{n2} \cdot i_n + L_{n2} \cdot \frac{\mathrm{d}i_n}{\mathrm{d}t} + U_{TO} + Z \cdot n \cdot i_n = 0. \quad (35)$$

The solution yields the time-dependent waveform of the desired current, expressed by the following equation:

$$i_n = \frac{U - U_{TO}}{R_{n2} + n \cdot Z} \left(1 - e^{-\frac{R_{n2} + n \cdot Z}{L_{n2}} \cdot t}\right) + I_2 e^{-\frac{R_{n2} + n \cdot Z}{L_{n2}} \cdot t}. \quad (36)$$

By substituting the time variable $t = t_{off} = (1–z)/f$, the expression for the current i_n with a magnitude of I_1 is obtained, as shown in Fig. 18:

$$I_1 = \frac{U - U_{TO}}{R_{n2} + n \cdot Z} \left(1 - e^{-\frac{R_{n2} + n \cdot Z}{L_{n2}} \cdot \frac{1-z}{f}}\right) + I_2 e^{-\frac{R_{n2} + n \cdot Z}{L_{n2}} \cdot \frac{1-z}{f}}. \quad (37)$$

Based on (31) and (37), expressions for the initial values of currents I_1 and I_2 at the beginning of both converter intervals can be derived, with these values determined solely by the circuit parameters. The current I_2 from (31) is substituted into (37):

$$I_1 = \frac{U - U_{TO}}{R_{n2} + n \cdot Z} \cdot \left(1 - e^{-\frac{R_{n2} + n \cdot Z}{L_{n2}} \cdot \frac{1-z}{f}}\right) + \\ + \left(\frac{U}{R_{n1}} \cdot \left(1 - e^{-\frac{R_{n1}}{L_{n1}} \cdot \frac{z}{f}}\right) + I_1 e^{-\frac{R_{n1}}{L_{n1}} \cdot \frac{z}{f}}\right) \cdot e^{-\frac{R_{n2} + n \cdot Z}{L_{n2}} \cdot \frac{1-z}{f}}. \quad (38)$$

The final expression for the current I_1 is obtained by rearranging (38) in the following form:

$$I_1 = \frac{\left(\frac{U - U_{TO}}{R_{n2} + n \cdot Z} \cdot \left(1 - e^{-\frac{R_{n2} + n \cdot Z}{L_{n2}} \cdot \frac{1-z}{f}}\right) + \right.}{\left. + \frac{U}{R_{n1}} \cdot \left(1 - e^{-\frac{R_{n1}}{L_{n1}} \cdot \frac{z}{f}}\right) \cdot e^{-\frac{R_{n2} + n \cdot Z}{L_{n2}} \cdot \frac{1-z}{f}}\right)} \\ \left(1 - e^{-\frac{R_{n1}}{L_{n1}} \cdot \frac{z}{f}} \cdot e^{-\frac{R_{n2} + n \cdot Z}{L_{n2}} \cdot \frac{1-z}{f}}\right) \quad (39)$$

The expression for the current I_2 is obtained by substituting (39) into (31).

Based on (30), (36), (39), (40), the time-dependent current waveform for any branch of a multi-branch buck-boost converter in boost mode can be expressed.

By considering the standard waveforms of the switching-on and switching-off processes, along with equation (1), the total losses P_C of the converter can be expressed similarly to the buck mode, as given in (19):

$$I_2 = \frac{U}{R_{n1}} \cdot \left(1 - e^{-\frac{R_{n1}}{L_{n1}} \cdot \frac{z}{f}}\right) + \\ + \frac{\left(\frac{U - U_{TO}}{R_{n2} + n \cdot Z} \cdot \left(1 - e^{-\frac{R_{n2} + n \cdot Z}{L_{n2}} \cdot \frac{1-z}{f}}\right) + \right.}{\left. + \frac{U}{R_{n1}} \cdot \left(1 - e^{-\frac{R_{n1}}{L_{n1}} \cdot \frac{z}{f}}\right) \cdot e^{-\frac{R_{n2} + n \cdot Z}{L_{n2}} \cdot \frac{1-z}{f}}\right)} \\ \left(1 - e^{-\frac{R_{n1}}{L_{n1}} \cdot \frac{z}{f}} \cdot e^{-\frac{R_{n2} + n \cdot Z}{L_{n2}} \cdot \frac{1-z}{f}}\right) \cdot e^{-\frac{R_{n1}}{L_{n1}} \cdot \frac{z}{f}}. \quad (40)$$

The average current of a converter branch can be determined using (20). Using this, the total losses of the converter can be expressed as:

$$P_C = nR_{Pn1}\left(I_{n(AV)}\right)^2 + nr_{DS\_1(on)}\left(I_{n(AV)}\right)^2 + nR_{Ln}\left(I_{n(AV)}\right)^2 + \\ + nr_{DS\_2(on)}z\left(I_{n(AV)}\right)^2 + nr_{DS\_2(off)}I^2_{DS(off)}(1-z) + \\ + nR_{Pn2}\left(I_{n(AV)}\right)^2(1-z) + n\left(U_{TO} + r_F\left(I_{n(AV)}\right)\right)I_{n(AV)}(1-z) + \\ + nUI_R + 0{,}5nU_{DS(on)}I_1t_{on}f + 0{,}5nU_{DS(off)}I_2t_ff + \\ + 0{,}5nQ_{rr}U_{DS(on)}f + 0{,}5nU_{FP}I_2t_{fr}f, \quad (41)$$

where $U_{DS(on)}$ is the voltage across the transistor just before it turns on, which can be expressed using (42); $U_{DS(off)}$ is the voltage across the transistor that increases shortly after it turns off, which can be expressed using (43):

$$U_{DS(on)} = U_{TO} + I_1 \cdot (r_F + R_{Pn2} + Z); \quad (42)$$

$$U_{DS(off)} = U_{TO} + I_2 \cdot (r_F + R_{Pn2} + Z). \quad (43)$$

By manipulating (41) and applying (20), a simplified final form of the relationship is obtained, which can be used to calculate the total losses in the converter:

$$P_C = \left(\frac{I^2}{n}\right)\cdot\left(R_{Pn1} + r_{DS\_1(on)} + R_{Ln} + r_F(1-z) + r_{DS\_2(on)}z + R_{Pn2}(1-z)\right) + \\ + nr_{DS\_2(off)}I^2_{DS(off)}(1-z) + nUI_R + U_{TO}I(1-z) + \\ + 0{,}5nU_{DS(on)}I_1t_{on}f + 0{,}5nU_{DS(off)}I_2t_ff + 0{,}5nQ_{rr}U_{DS(on)}f + \\ + 0{,}5nU_{FP}I_2t_{fr}f. \quad (44)$$

The efficiency of the converter is given by (23). From (23), it is evident that the dominant factor affecting efficiency is the total loss power. The magnitude of these losses can be influenced by the appropriate selection of individual design components. Additionally, the total losses can be affected by the number of parallel branches in the converter, as the input current is linearly divided among the branches, while the losses in the branch resistors decrease quadratically. Therefore, the total losses may be smaller with multiple branches than with a single branch. However, due to additional losses in the parallel branches, it is not necessarily true that a greater number of branches will always result in lower losses. Given these considerations, it is possible to determine the optimal number of branches for the desired input power (under constant input voltage, for the desired input current, and thus for a specific duty cycle) in the boost mode. The converter can, therefore, be controlled by adjusting the topology and duty cycle to achieve the highest possible efficiency for any given input power. This is, of course, under the condition of fixed design components and their characteristics.

To determine the optimal number of branches, equation (44) must be differentiated. By differentiating it with respect to n, the result for the local extremum can be obtained, providing an expression for the number of branches corresponding to the minimum loss power:

$$P'_C = -\left(\frac{I^2}{n}\right)\cdot\left(R_{Pn1} + r_{DS\_1(on)} + R_{Ln} + r_F(1-z) + r_{DS\_2(on)}z + R_{Pn2}(1-z)\right) + \\ + zUI_R + r_{DS\_2(off)}I^2_{DS(off)}(1-z) + 0{,}5U_{DS(on)}I_1t_{on}f + \\ + 0{,}5U_{DS(off)}I_2t_ff + 0{,}5Q_{rr}U_{DS(on)}f + 0{,}5U_{FP}I_2t_{fr}f. \quad (45)$$

If the result of the differentiation is set equal to zero and solved for n, the equation takes the following form:

$$n = I\sqrt{\frac{\left(\begin{array}{l} R_{Pn1} + r_{DS\_1(on)} + R_{Ln} + r_F(1-z) + \\ + r_{DS\_2(on)}z + R_{Pn2}(1-z) \end{array}\right)}{\left(\begin{array}{l} zUI_R + r_{DS\_2(off)}I^2_{DS(off)}(1-z) + 0{,}5U_{DS(on)}I_1t_{on}f + \\ + 0{,}5U_{DS(off)}I_2t_ff + 0{,}5Q_{rr}U_{DS(on)}f + 0{,}5U_{FP}I_2t_{fr}f \end{array}\right)}}. \quad (46)$$

It follows from the above that, based on (46), the optimal number of branches can be determined using the design and operating parameters of the converter in boost mode, ensuring that the converter delivers the maximum power to the load under all operating conditions. The validity of the formula for the buck mode has also been experimentally confirmed. A comparison of the results obtained through calculation and measurement is presented in Table 2. For the boost mode, the same circuit parameters were used, except for the input power source and load. In this case, the calculation was performed with a 10 V power supply and a 20 Ω load.

Table 2

Efficiency results of the boost converter mode as a function of power and the number of branches

Single-phase converter in boost mode			
Calculated		Measured	
P_1, W	Efficiency, %	P_1, W	Efficiency, %
5,03	92,95	5,05	92,25
10,03	93,91	10,05	93,49
15,02	93,5	15,08	93,10
20,02	92,58	20,06	92,22
30,03	90,25	30,07	89,83
40,06	87,66	40,08	87,14
50,04	84,99	50,06	84,38
Three-phase converter in boost mode			
Calculated		Measured	
P_1, W	Efficiency, %	P_1, W	Efficiency, %
5,05	90,7	5,01	89,65
10,04	93,2	10,05	92,71
15,01	94,2	15,02	93,72
20,07	94,7	20,05	94,12
30,05	94,93	30,09	94,38
40,08	94,5	40,00	93,97
50,01	93,85	50,04	93,15

To provide a clearer understanding of the obtained results, a graph has been created (Fig. 19).

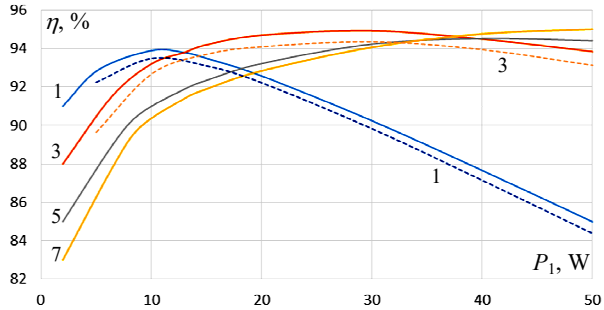

Fig. 19. Graphical representation of the efficiency results as a function of input power and the number of branches (1, 3, 5, 7), obtained through calculations (—) and measurement (- - -)

To further illustrate the implications of the calculations, Fig. 20 depicts the calculated dependence of the efficiency of a converter operating in boost mode on its output power.

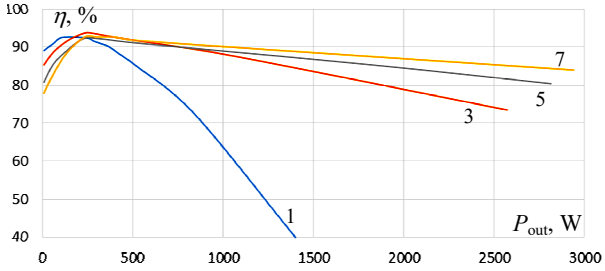

Fig. 20. Graphical representation of the efficiency results as a function of output power and the number of branches (1, 3, 5, 7), obtained through calculations for higher power converter

This analysis pertains to a higher-power converter implemented with the components and circuit parameters described in the preceding text.

Conclusions. Based on the obtained equations, as well as the presented waveforms, several critical factors influencing the optimal design and operation of multi-branch buck-boost converters can be identified. The analysis reveals that for operating points of a buck-boost converter functioning in buck mode with power input up to approximately 10 % of the installed power capacity (P_1), a single-branch configuration is more efficient than a seven-branch configuration. At 10 % of P_1, the efficiency difference between these configurations can reach up to 10 %. For a converter with an installed power capacity of, for instance, 3 kW, this efficiency gap could result in operational losses of up to 300 W. A similar situation arises for operating points of the buck-boost converter operating in boost mode. However, in this case, the single-branch configuration demonstrates a clear efficiency advantage only for power input levels up to approximately 6 % of the total installed capacity. Within this range, the single-branch configuration remains up to 10 % more efficient than the seven-branch configuration. It is important to note, however, that the absolute magnitude of the converter's losses is influenced not only by the number of branches but also by the parameters of the components used in the circuit.

Conflict of interest. The authors declare that they have no conflicts of interest.

REFERENCES

1. Alharbi M.A., Dahidah M.S.A., Ali S.A., Ethni S.A.E., Pickert V. Ripple-Free Multiphase Interleaved Stacked Converter for High-Power Applications. *IEEE Transactions on Power Electronics*, 2022, vol. 37, no. 12, pp. 14770-14780. doi: https://doi.org/10.1109/TPEL.2022.3194979.

2. Hafeez K.T., Dutta A., Singh S.G., Avalur K.K.G. A low-cost multi-phase 3A buck converter with improved ripple cancellation for wide supply range. *2016 IEEE International Symposium on Circuits and Systems (ISCAS)*, 2016, pp. 1618-1621. doi: https://doi.org/10.1109/ISCAS.2016.7538875.

3. Rahman A.U., Pellitteri F., Campagna N., Di Tommaso A.O., Miceli R. Current Sharing Control of Multiphase Interleaving Single Inductor Four Switch Buck-Boost Converter for Energy Storage System. *2024 IEEE 15th International Symposium on Power Electronics for Distributed Generation Systems (PEDG)*, 2024, pp. 1-6. doi: https://doi.org/10.1109/PEDG61800.2024.10667462.

4. Li J., Zhang L., Wu X., Zhou Z., Dai Y., Chen Q. Current Estimation and Optimal Control in Multiphase DC–DC Converters With Single Current Sensor. *IEEE Transactions on Instrumentation and Measurement*, 2024, vol. 73, pp. 1-14, art. no. 9003414. doi: https://doi.org/10.1109/TIM.2024.3396834.

5. Tang J., Guo T., Kim J.S., Roh J. A Current-Mode Four-Phase Synchronous Buck Converter With Dynamic Dead-Time Control. *IEEE Access*, 2021, vol. 9, pp. 81078-81088. doi: https://doi.org/10.1109/ACCESS.2021.3085826.

6. Golla T., Kapat S., Chittaragi N., Setty R.A., Sridharan S. Controller Design and Phase Current Balancing for Fast Dynamic Performance in Voltage Mode Controlled Multiphase Buck Converters. *2023 IEEE Applied Power Electronics Conference and Exposition (APEC)*, 2023, pp. 2163-2169. doi: https://doi.org/10.1109/APEC43580.2023.10131482.

7. Wang L., Zhang D., Duan J., Gu R. Research on High-Performance Multiphase DC–DC Converter Applied to Distributed Electric Propulsion Aircraft. *IEEE Transactions on Transportation Electrification*, 2023, vol. 9, no. 3, pp. 3545-3563. doi: https://doi.org/10.1109/TTE.2022.3207142.

8. Ayada A., Guiza D., Ounnas D., Tidjani N. Design and control of a DC-DC buck converter using discrete Takagi-Sugeno fuzzy models. *Electrical Engineering & Electromechanics*, 2025, no. 3, pp. 53-58. doi: https://doi.org/10.20998/2074-272X.2025.3.08.

9. Namoune A., Taleb R., Mansour N., Benzidane M.R., Boukortt A. Integrated through-silicon-via-based inductor design in buck converter for improved efficiency. *Electrical Engineering & Electromechanics*, 2023, no. 6, pp. 54-57. doi: https://doi.org/10.20998/2074-272X.2023.6.09.

10. Nguyen V.H., Do X.-D., Blaquiere Y., Cowan G. Multi-Phase Hybrid Boost Converter with High Conduction Loss Reduction and Fast Dynamic Response for Automotive Applications. *2022 20th IEEE Interregional NEWCAS Conference (NEWCAS)*, 2022, pp. 183-187. doi: https://doi.org/10.1109/NEWCAS52662.2022.9842223.

11. Deshmukh N., Prabhakar S., Anand S. Power Loss Reduction in Buck Converter Based Active Power Decoupling Circuit. *IEEE Transactions on Power Electronics*, 2021, vol. 36, no. 4, pp. 4316-4325. doi: https://doi.org/10.1109/TPEL.2020.3024721.

12. Kandeel Y., O'Driscoll S., O'Mathuna C., Duffy M. Optimum Phase Count in a 5.4-W Multiphase Buck Converter Based on Output Filter Component Energies. *IEEE Transactions on Power Electronics*, 2023, vol. 38, no. 4, pp. 4909-4920. doi: https://doi.org/10.1109/TPEL.2022.3226708.

13. Yama O., Khyzhniak T., Bondarenko O. Analysis of Modified Non-Isolated DC-DC Converters and Solutions to Improve their Characteristics. *2023 IEEE 4th KhPI Week on Advanced Technology (KhPIWeek)*, 2023, pp. 1-6. doi: https://doi.org/10.1109/KhPIWeek61412.2023.10312965.

14. Azer P., Emadi A. Generalized State Space Average Model for Multi-Phase Interleaved Buck, Boost and Buck-Boost DC-DC Converters: Transient, Steady-State and Switching Dynamics. *IEEE Access*, 2020, vol. 8, pp. 77735-77745. doi: https://doi.org/10.1109/ACCESS.2020.2987277.

15. Hinov N., Hranov T. Model-Based Optimisation of a Buck-Boost DC-DC Converter. *2020 21st International Symposium on Electrical Apparatus & Technologies (SIELA)*, 2020, pp. 1-5. doi: https://doi.org/10.1109/SIELA49118.2020.9167056.

16. Lyu Y., Sanusi B.N., Ouyang Z. Modeling and Analysis of Coupling Effect in Four Legged Core for Multi-phase Buck Converter. *2023 IEEE Applied Power Electronics Conference and Exposition (APEC)*, 2023, pp. 3307-3313. doi: https://doi.org/10.1109/APEC43580.2023.10131131.

17. Sridhar S., Li Q. Multiphase Constant On-Time Control With Phase Overlapping – Part I: Small-Signal Model. *IEEE Transactions on Power Electronics*, 2024, vol. 39, no. 6, pp. 6703-6720. doi: https://doi.org/10.1109/TPEL.2024.3368343.

18. Lu X., Yin X., Zhuo C. An Efficient Approach to Multiphase Constant On-Time Buck Converter Simulation. *2024 2nd International Symposium of Electronics Design Automation (ISEDA)*, 2024, pp. 143-148. doi: https://doi.org/10.1109/ISEDA62518.2024.10617689.

19. Hamdi R., Hadri Hamida A., Bennis O. On modeling and real-time simulation of a robust adaptive controller applied to a multicellular power converter. *Electrical Engineering & Electromechanics*, 2022, no. 6, pp. 48-52. doi: https://doi.org/10.20998/2074-272X.2022.6.08.

20. Zagirnyak M., Kalinov A., Maliakova M. Analysis of instantaneous power components of electric circuit with a semiconductor element. *Archives of Electrical Engineering*, 2013, vol. 62, no. 3, pp. 473-486. doi: https://doi.org/10.2478/aee-2013-0038.

21. Jacko P., Bereš M., Kováčová I., Molnár J., Vince T., Dziak J., Fecko B., Gans Š., Kováč D. Remote IoT Education Laboratory for Microcontrollers Based on the STM32 Chips. *Sensors*, 2022, vol. 22, no. 4, art. no. 1440. doi: https://doi.org/10.3390/s22041440.

22. Kulshreshtha A., Saxena A.R., Veerachary M. Non-Isolated Fourth-Order Boost DC-DC Converter for Power Management in Low Voltage Low Power DC Grids: Design and Interaction Analysis. *IEEE Access*, 2020, vol. 8, pp. 196500-196514. doi: https://doi.org/10.1109/ACCESS.2020.3034181.

Received 27.12.2024
Accepted 04.02.2025
Published 02.07.2025

I. Kovacova[1], *Professor,*
D. Kovac[1], *Professor,*
[1] Technical University of Kosice,
Department of Theoretical and Industrial Electrical Engineering,
Park Komenskeho 3, 042 00 Kosice, Slovakia,
e-mail: irena.kovacova@tuke.sk;
dobroslav.kovac@tuke.sk (Corresponding Author)

How to cite this article:
Kovacova I., Kovac D. Designing the optimal number of active branches in a multi-branch buck-boost converter. *Electrical Engineering & Electromechanics*, 2025, no. 4, pp. 44-52. doi: https://doi.org/10.20998/2074-272X.2025.4.06